



HAL
open science

Downstream erosion and deposition dynamics of fine suspended sediments due to dam flushing

G. Antoine, B. Camenen, M. Jodeau, J. Némery, M. Esteves

► **To cite this version:**

G. Antoine, B. Camenen, M. Jodeau, J. Némery, M. Esteves. Downstream erosion and deposition dynamics of fine suspended sediments due to dam flushing. *Journal of Hydrology*, 2020, 585 (5), pp.124763. 10.1016/j.jhydrol.2020.124763 . hal-03118381

HAL Id: hal-03118381

<https://hal.science/hal-03118381>

Submitted on 22 Jan 2021

HAL is a multi-disciplinary open access archive for the deposit and dissemination of scientific research documents, whether they are published or not. The documents may come from teaching and research institutions in France or abroad, or from public or private research centers.

L'archive ouverte pluridisciplinaire **HAL**, est destinée au dépôt et à la diffusion de documents scientifiques de niveau recherche, publiés ou non, émanant des établissements d'enseignement et de recherche français ou étrangers, des laboratoires publics ou privés.

1 Downstream erosion and deposition dynamics of fine
2 suspended sediments due to dam flushing

3 G. Antoine^{a,b}, B. Camenen^c, M. Jodeau^{a,b}, J. Némery^d, M. Esteves^d

4 ^aEDF-LNHE, 6 Quai Watier, 78400 Chatou, France

5 ^bLHSV -Laboratoire Hydraulique St Venant-, 6 Quai Watier, 78400 Chatou, France

6 ^cINRAE, UR RiverLy, centre de Lyon-Grenoble, 5 Rue de la Doua, CS 20244, 69625
7 Villeurbanne Cedex, France

8 ^dIGE -Université Grenoble Alpes, CNRS, IRD, Grenoble INP (Institute of Engineering
9 Univ. Grenoble Alpes)-, 38000 Grenoble, France

10 **Abstract**

11 Fine sediment dynamics downstream dams is a key issue when dealing
12 with environmental impact of hydraulic flushing. This paper presents an
13 analysis of six field campaigns carried out during dam flushing events (in
14 June 2006, 2007, 2009, 2010, 2011, and 2012) in the Arc- Isère river system
15 in the Northern French Alps. Suspended sediment concentrations (SSC) and
16 discharges were evaluated using direct measurements or/and 1D hydraulic
17 modelling at up to 14 locations along the 120 kilometres-long river channel.
18 The total suspended sediment flux (SSF) is analysed along the Arc and Isère
19 rivers for each Arc dam flushing event. Uncertainties were quantified based
20 on a propagation method of both measurement and modelling errors. The
21 resulting confidence interval provides elements of discussion on the signifi-
22 cance of the sediment mass balance between two consecutive measurement
23 sites. Whereas the discharge time-series of each flushing event is roughly
24 the same, the quantity of fine sediments removed from the reservoirs varied
25 from 10,000 tons in 2007 to 40,000 tons in 2006. Also, a significant erosion is
26 observed in the river system for some events (20,000 tons in 2007) while the
27 SSF barely varied for other events (in 2009 and 2011). This detailed data set
28 allows to identify specific locations in the river network where deposition or
29 erosion occurred. This dynamics is closely related to both the hydrology in
30 the upper Isère River and the morphology of the Arc and Isère rivers, which
31 have been affected by the 2008 and 2010 floods.

32 *Keywords:*

33 dam flushing, impounded Alpine river, suspended sediment concentration
34 (SSC), suspended sediment flux, local mass balance

35 **1. Introduction**

36 About 1% of the total storage capacity in the world's reservoirs is lost each
37 year due to sedimentation (Mahmood, 1987; Yoon, 1992; Vörösmarty et al.,
38 2003). This sedimentation rate depends mainly on the size of the reservoir re-
39 lative to the amount of sediment flowing into it. Since the construction of new
40 dams is rather difficult in developed countries due to stricter environmental
41 regulations and the lack of suitable sites, procedures have been established
42 to sustain the storage capacity of existing reservoirs. In numerous cases, hy-
43 draulic flushing has been used successfully to restore lost reservoir storage
44 capacity (Kondolf et al., 2014). The flushing process consists in opening dam
45 outlet gates to produce flows with velocities high enough to flush away the
46 sediments accumulated in the reservoir. Theoretical and numerical studies
47 (Chang et al., 1996; Olsen, 1999; Liu et al., 2004; Khosronejad et al., 2008; Ji
48 et al., 2011), laboratory experiments (Lai and Shen, 1996; Campisano et al.,
49 2004, 2008), and field observations (Jansson and Erlingsson, 2000; Rayan
50 and Iguacel, 2006) have shown that under appropriate conditions, hydraulic
51 flushing can remove both fine (with cohesive material) and coarse (sands and
52 gravels) sediments.

53 Flushing operations can have a significant impact on the morphology and
54 ecology of the downstream part of a river system (Collier, 2002; Chung et al.,
55 2008; Crosa et al., 2010; Bilotta et al., 2012; Alcayaga et al., 2018). As an
56 example, Crosa et al. (2010) observed a drop in trout density as high as 73%
57 a flushing operation performed in 2006 in an alpine reservoir. In this case,
58 high suspended sediment concentrations (SSC) were measured in the down-
59 stream part of the river (peak values up to 80 g/l and event-averaged value
60 equal to 4 g/l). On the other hand, when limits for SSC are adopted, Pe-
61 teuil et al. (2013); Espa et al. (2015, 2019) demonstrated that environmental
62 degradations can be significantly reduced. Also, several studies have focused
63 on the morphological effect of flushing waves on the river bed, which mainly
64 concerns coarse sediments (Kondolf and Wilcock, 1996; Wohl and Cenderelli,
65 2000; Brandt, 2000; Petts and Gurnell, 2005; Petticrew et al., 2007). These
66 studies identified the direct link existing between the intensity of the flushing
67 operations and the downstream erosion of the river bed (gravel bars or main
68 channel).

69 However, fine sediments transported by flushing flows can also have a
70 morphological impact on the downstream river system (Smart, 1999; Van
71 Maren et al., 2010). Following a flushing event, Brandt (1999) measured an
72 increase of mean bed elevation of 10 centimetres due to the deposition of fine
73 sediments over a 30 kilometre-long reach downstream of the Cachi dam, in
74 Costa Rica. As an exacerbating factor, vegetation grows more easily on fine
75 deposits, and provides optimal conditions for new deposition of fine sediments
76 due to the local decrease of flow velocities (Newcombe and Macdonald, 1991;
77 Murle et al., 2003; Asaeda and Rashid, 2012; Jourdain et al., 2017). Finally,
78 fine sediments can be the vectors of propagation for particulate pollutants,
79 and the residence time of the contaminated particles in the river channel is
80 an important parameter to evaluate the vulnerability of a system (Frémion
81 et al., 2016).

82 Fine sediment deposition fluxes often represent a small part of the total
83 suspended sediment flux (SSF) in embanked alpine river for high flow condi-
84 tions. They have been observed as non-negligible for small braided systems
85 only (Navratil et al., 2010; Misset et al., 2019), where exchanges with the
86 bed can be of the same order of magnitude than upstream input. There-
87 fore, the quantification of the mass of fine deposited sediments, its spatial
88 distribution and its temporal dynamics during one event is rather difficult
89 to assess for large embanked systems. Bathymetric surveys performed before
90 and after a flushing event are expensive, time consuming and highly exposed
91 to uncertainty measurement regarding the possibly small thickness of fine
92 sediment deposits. Some aerial photograph analysis provided an estimate of
93 the deposits but limited to surface measurements and difficult to apply to
94 long reaches (Camenen et al., 2013; Camenen et al., 2016). Furthermore, the
95 measured bed evolution provides an estimation of the volume of sediments
96 deposited or eroded. To be compared to sediment fluxes, an additional hy-
97 pothesis on the sediment mixture and porosity of the bed is needed to convert
98 the differential volume into a sediment mass.

99 The method based on SSF consists in estimating the difference between
100 event-integrated SSF for two consecutive positions of the river reach. Such
101 method only provides a reach-averaged behaviour that could be difficult to
102 interpret if the distance between two positions is long. Moreover, the un-
103 certainty is sensitive to the temporal frequency of measurements, and can
104 sometimes become too high to give relevant conclusions (Garcia, 2008). This
105 explains that few studies have focused on fine sediment budgets based on SSF
106 measurements, especially for long embanked systems (López-Tarazón et al.,

107 2012). None of these studies quantified precisely or examined critically their
108 results with respect to uncertainty values. As an example, the work of Tena
109 et al. (2014) on the Ebro River improves the understanding of the spatial and
110 temporal dynamics of suspended sediment transport during flushing flow but
111 it did not address the issue of fine sediment deposition in the river.

112 In this paper we raise the following questions: what is the downstream
113 dynamics of SSF during dam flushing events in an impounded river system?
114 Regarding the uncertainty on SSF estimated from a detailed data set, what
115 is the significance of local mass balance between two consecutive measure-
116 ment sites? How to explain these mass balances with erosion and deposition
117 processes on the river bed? To answer these questions, we analysed the prop-
118 agation of SSF along the Arc and Isère river system following six hydraulic
119 flushing events of the Upper Arc dams in June 2006, 2007, 2009, 2010, 2011,
120 and 2012. For these six flushing events, measurements of discharges and SSC
121 were performed at fourteen sites along 120 kilometres of the river downstream
122 of the flushed reservoirs (Antoine, 2013).

123 In the first part of this paper we describe the field campaigns performed
124 to measure water discharges and SSC at different sites of the river system as
125 well as the method developed to explore this detailed data set. The obtained
126 instantaneous values of SSF are integrated over the flushing time period, in
127 order to compute the local mass balances between two consecutive measure-
128 ment sites. Then, a model of uncertainty propagation is proposed to estimate
129 the significance of these local mass balances. In the second part of the paper,
130 a global analysis of discharge, SSC and SSF values is provided at the river
131 scale. Also, a discussion is provided on the links between local mass balances
132 and site morphologies and history.

133 **2. Material and method**

134 *2.1. Study site*

135 The Arc-Isère river system is a typical example of impounded Alpine river
136 system largely influenced by river management and dam management.

137 *2.1.1. The Arc-Isère River system*

138 The Isère River and its tributary, the Arc River, are located in the North-
139 ern French Alps. The respective surface areas of the catchments are 1950 km²
140 and 5570 km² for the Arc River and the Isère River upstream of the city of

141 Grenoble (Figure 1). Both catchments are characterized by a nival hydro-
142 logical regime, with an annual mean water discharge of $30 \text{ m}^3/\text{s}$ for the Arc
143 River at Pontamafrey and $177 \text{ m}^3/\text{s}$ for the Isère River at Grenoble.

144 In the second part of the 20th century, three dams, with a storage ca-
145 pacity of 0.8 Mm^3 , were built on the middle section of the Arc River: the
146 Freney dam, the Pont-des-Chèvres dam and the Saint-Martin-la-Porte dam
147 (SMLP dam). Compensation water flows along more than 50% of the to-
148 tal length of the Arc River due to the water intakes used for hydropower
149 generation. Nevertheless, tributaries of the Arc and Isère rivers can be very
150 dynamic, and strong seasonal discharge variations occur in both rivers dur-
151 ing the year: in the middle of summer, the mean monthly discharges on the
152 lower Arc River can reach $50 \text{ m}^3/\text{s}$, and $250 \text{ m}^3/\text{s}$ on the Isère River. In
153 winter, mean monthly discharges are $10 \text{ m}^3/\text{s}$ on the Arc River and $150 \text{ m}^3/\text{s}$
154 on the Isère River. Natural floods usually occur at the beginning of summer
155 and in autumn. Dams are opened during large floods and have no impact
156 on the flood dynamics in the downstream part of the valley because of their
157 low storage capacities (Marnezy, 1999). The discharge for the 10-years flood
158 on Arc River (Pontamafrey) is estimated at $180 \text{ m}^3/\text{s}$, and $900 \text{ m}^3/\text{s}$ on the
159 Isère River (Grenoble).

160 Because of continuous embankments, the Arc River is strongly constrained
161 laterally and the mean slope of the river bed varies from 1% at Saint-Jean-
162 de-Maurienne to 0.2% just upstream of its confluence with the Isère River.
163 The slope can be locally steeper and supercritical flows are frequently ob-
164 served on some parts of the river's course. The slope of the Isère River is
165 smaller, with values from 0.2% close to the confluence to 0.09% at the end
166 of the study site. Both Arc and Isère river beds are mainly made of gravels
167 with a poorly sorted grain size distribution. Both rivers are characterized by
168 systems of alternate bars that are often vegetated in the Isère River (Serlet
169 et al., 2018). They are also exposed to snow-melt floods, debris flows and
170 are greatly affected by deposits of fine sediment on vegetated banks. This
171 paper focuses on the Arc-Isère river system, from the SMLP dam to the city
172 of Grenoble. The locations of the measurement sites are defined in this paper
173 as the distance of the site from the confluence (sites on the Arc River have
174 negative positions and sites on the Isère River have positive positions).

175 *2.1.2. Flushing of the Arc dams*

176 To maintain storage capacity and electric power production, the three
177 dams of the middle Arc River (Figure 1) are flushed yearly at the beginning

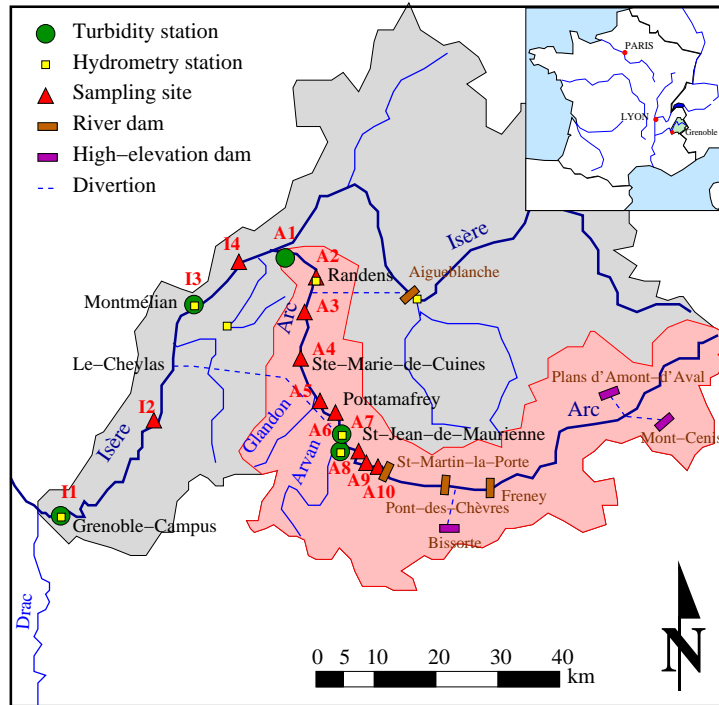


Figure 1: Map showing the location of the Arc and Isère catchments and measurement sites.

178 of June, except if a larger flood occurs before the planned hydraulic flush-
 179 ing. For example, no flush was performed in 2008 because a 15-years flood
 180 occurred in May. During the flushing operation, the successive openings of
 181 the dam outlet gates (see Figure 2a) are defined precisely to optimize the
 182 hydraulic effect of the flush. As dam operators follow a project hydrograph,
 183 similar discharge time series were observed for every flushing event (see Fig-
 184 ure 2b) although some differences can be observed because of the natural flow
 185 in the Arc and Isère rivers. At the SMLP dam, the different dam opening
 186 phases correspond to the following parts of the hydrograph in the Arc River:

- 187 1. first a warning wave (for fauna and hydraulic safety precautions) of
 188 about $20 \text{ m}^3/\text{s}$ is generated by an overflow of the clear water;
- 189 2. then a discharge step is performed, providing a discharge amplitude of
 190 approximately $90 \text{ m}^3/\text{s}$ for 3 hours;
- 191 3. water is provided by larger reservoirs on the upper Arc watershed (Bis-
 192 sorte and Mont-Cenis dam reservoirs mainly, see Fig. 1) to maintain

193 the water discharge value and increase it to its maximum value (from
 194 130 to 150 m³/s) for about 4 hours. The maximum discharge value
 195 corresponds to a one-year flood on the Arc River;
 196 4. the discharge returns to the compensation water level.

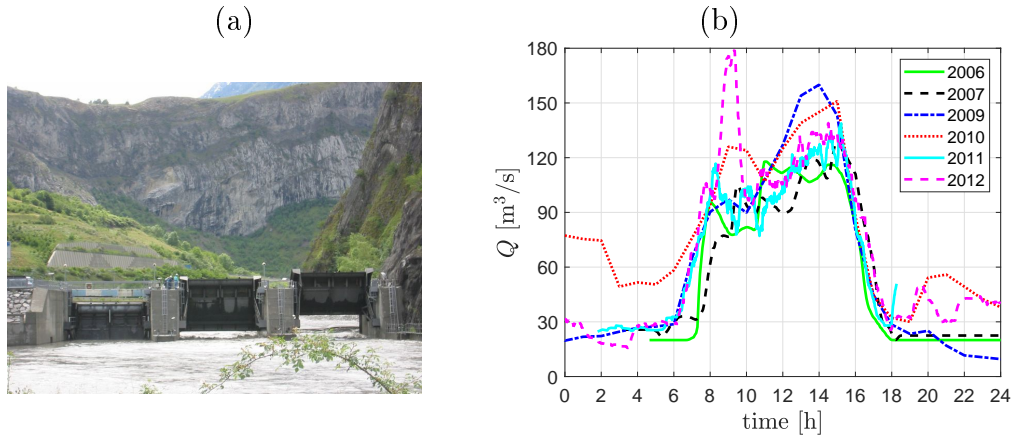


Figure 2: Photo of the SMLP dam outlet gates during a flushing event (a), and discharge time series of the six studied flushing events at Pontamafrey (b).

197 In 2012, an additional peak up to 175 m³/s arose during the first discharge
 198 step. It resulted from some unexpected problems in the gate management.

199 2.2. SSC and discharge measurements

200 To evaluate the suspended load propagation along the reach resulting
 201 from dam flushing events, high frequency measurements were performed dur-
 202 ing June 2006, 2007, 2009, 2010, 2011, and 2012 events. These measurements
 203 were anticipated and organization was facilitated by planning the dam flush-
 204 ing several weeks in advance. Measurements consisted in gauging discharges
 205 and performing SSC monitoring at several locations along the river reach
 206 (Figure 1).

207 SSCs were estimated from samples taken from surface water (bucket sam-
 208 ples from a bridge) or at the riverside (ISCO 4230 automatic sampler) at 14
 209 measurement sites (Figure 1). The samples were filtered and weighed follow-
 210 ing the ISO 11923 protocol. SSC estimation was also performed thanks to
 211 turbidimeters (Hach Lange Solitax SC-Line TS 50 g/l) installed at four moni-
 212 toring stations (Thollet et al., 2018). In these cases, water samples were used
 213 to establish a relation between the measured turbidity and the effective SSC.

214 As a consequence, it is important to note that the present study excludes
215 coarse particles such as sand since it is poorly measured from surface and/or
216 riverside samples and turbidity. In addition, samples were taken in main trib-
217 utaries (Arvan, Glandon, Isère restitution, Isère River) to verify that their
218 concentrations were negligible throughout the flushing events. Therefore, the
219 only effect of these tributaries was to decrease the SSC through dilution.

220 Discharges were estimated at five sites along the Arc-Isère system (A7,
221 A5, A2, I3, and I1) where a hydrometric station is present. At these sites, wa-
222 ter level was measured and the discharge was obtained using well documented
223 rating curves and additional discharge measurements (using a classical cur-
224 rent meter, LSPIV image analysis technique and/or ADCP measurements
225 Jodeau et al., 2008; Dramais et al., 2011). In addition, pressure gauges
226 (autonomous Diver type and bubbler system pressure gauges) were used to
227 measure water level variations at several locations, giving information on the
228 transfer time of the flushing waves.

229 One dimensional hydraulic model was built for the whole river system
230 to complete the discharge data set. The 1D hydraulic numerical code MAS-
231 CARET (Goutal and Maurel, 2002, part of the open-source TELEMAC-
232 MASCARET system) was used for this study. The model geometry was
233 built using topographical data from several river cross-section surveys con-
234 ducted between 2004 and 2007 on the Arc and Isère Rivers. 56 river cross
235 sections were available to build the Arc River bed, giving an average profile
236 density of about 1 cross section per kilometre. On the Isère River, this den-
237 sity was higher (about one profile every 200 meters). Because local slopes
238 can be very steep, the calculation mesh was fixed at spatial resolution of
239 20m. Calibration of the Strickler coefficients was performed by comparing
240 measured and computed water level and discharge values. Strickler friction
241 coefficients used to calibrate the model vary from 20 $\text{m}^{1/3}/\text{s}$ in the upstream
242 part to 45 $\text{m}^{1/3}/\text{s}$ in the downstream part.

243 The upstream boundary condition was built from the most upstream dis-
244 charge time-series measured on the river (A7, Figure 1) using a time shift
245 based on pressure gauge measurements. The downstream boundary condi-
246 tion is a free water flux boundary condition. Three main water inputs were
247 set at Randens (10 km upstream the Arc-Isère confluence; turbinated water
248 from the Aigueblanche reservoir), at the confluence (upstream part of the
249 Isère River), and at Cheylas (30 km downstream the Arc-Isère confluence;
250 turbinated water from the Flumet reservoir).

251 Table 1 summaries the measurement methods used at each measurement

252 site for each flushing event. The position of each measurement site is given
 253 by its distance from the confluence (see also Figure 1). Both SSCs and water
 254 discharge time series are thus available at 14 measurement sites for the five
 255 flushing events.

Table 1: Summary of the methods used for discharge and concentration measurements (Site: code of the measurement point located at the distance D from the confluence). Three methods were used for the concentration values (A.S.: Automatically Sampled, M.S.: Manually Sampled, Tu: Turbidity measurements) and two methods were used for the discharge values (H.S.: Discharge values from Hydrometric Stations, 1D: Discharge values computed with the 1D model).

Site	X [km]	2006	2007	2009	2010	2011	2012
		$SSC Q$	$SSC Q$	$SSC Q$	$SSC Q$	$SSQ Q$	$SSQ Q$
A10	-50.4	- -	M.S. 1D	M.S. 1D	M.S. 1D	M.S. 1D	M.S. 1D
A9	-48.5	M.S. 1D	M.S. 1D	- -	- -	- -	- -
A8	-44.7	M.S. 1D	M.S. 1D	M.S. 1D	M.S. 1D	M.S. 1D	- -
A7	-40.0	M.S. H.S.	Tu. H.S.	Tu. H.S.	Tu. H.S.	Tu. H.S.	Tu. H.S.
A6	-37.9	M.S. 1D	M.S. 1D	M.S. 1D	M.S. 1D	A.S. 1D	- -
A5	-33.1	M.S. H.S.	Tu. H.S.	Tu. H.S.	M.S. H.S.	M.S. H.S.	M.S. H.S.
A4	-24.0	- -	A.S. 1D	A.S. 1D	A.S. 1D	A.S. 1D	A.S. 1D
A3	-12.2	A.S. 1D	A.S. 1D	A.S. 1D	A.S. 1D	A.S. 1D	A.S. 1D
A2	-9.2	A.S. 1D	A.S. 1D	A.S. 1D	A.S. 1D	- H.S.	- H.S.
A1	-0.3	A.S. 1D	A.S. 1D	A.S. 1D	A.S. 1D	Tu 1D	Tu 1D
I4	3.6	A.S. 1D	A.S. 1D	A.S. 1D	- -	- -	- -
I3	13.8	- -	- -	- -	Tu. H.S.	Tu. H.S.	Tu. H.S.
I2	26.8	A.S. 1D	- -	- -	A.S. 1D	A.S. 1D	- -
I1	63.1	Tu. H.S.	Tu. H.S.	Tu. H.S.	Tu. H.S.	Tu. H.S.	Tu. H.S.

256 2.3. Suspended Sediment Fluxes

257 2.3.1. Instantaneous Suspended Sediment Fluxes

258 At each measurement site located at the position X_i , instantaneous flux
 259 values ϕ are computed using a linear interpolation of both discharges and
 260 SSC values:

$$\phi(X_i, t) = Q(X_i, t) \times SSC(X_i, t) \quad (1)$$

261 Due to a lack of data, three data sets were excluded: site I4 in 2006
 262 and 2007 and site A1 in 2007. SSC data were measured at site A2 with an
 263 automatic sampler. However, since this site is located 500 m downstream

264 the outlet channel of the Randens hydro-power plant, an incomplete lateral
 265 mixing was suspected. SSC measurements were performed at several points
 266 throughout the river in 2010; the results presented a standard deviation up
 267 to 40% due to incomplete lateral mixing, even under low SSC conditions.
 268 Consequently, no SSC measurement is made at this site since 2011, and the
 269 data from this site will be excluded from the flux estimations.

270 2.3.2. Suspended Sediment Fluxes integrated over the flushing event

271 The instantaneous flux computed using Eq. 1 can be integrated over the
 272 time period of the event T_{event} , which varies from 12 hours in the Arc River
 273 to 16 hours in the Isère River, due to dispersion processes:

$$\Phi(X_i) = \int_{T_{event}} \phi(X_i, t) dt \quad (2)$$

274 This temporal integration provides the global mass of suspended sediment
 275 Φ transported through a measurement site located at position X_i . A for-
 276 malism was also introduced to study the temporal dynamic. A cumulative
 277 transported mass was calculated as a function of the percentage $t\%$ of T_{event} :

$$\Phi_{\%}(X_i, t\%) = \int_{t\% \times T_{event}} \phi(X_i, t) dt \quad (3)$$

278 2.3.3. Local mass balance

279 The detailed spatial profiles of the total mass transported at the fourteen
 280 measurement sites are used to estimate a local mass balance. This local mass
 281 balance $\Delta\Phi$ between two consecutive measurement sites located at positions
 282 X_i and X_{i+1} , respectively, is expressed such as:

$$\Delta\Phi(i \rightarrow i + 1) = \Phi(X_{i+1}) - \Phi(X_i) \quad (4)$$

283 This integrated approach could mask successive deposition or erosion
 284 phases during one event. Then, it is possible to obtain a dynamic local
 285 mass balance value using Eq. 3, i.e. a mass balance between two consecutive
 286 measurement sites after $t\%$ of T_{event} :

$$\Delta\Phi_{\%}(i \rightarrow i + 1, t\%) = \Phi_{\%}(X_{i+1}, t\%) - \Phi_{\%}(X_i, t\%) \quad (5)$$

287 Note that $\Phi(X_i) = \Phi_{\%}(X_i, 100\%)$ and $\Delta\Phi(i \rightarrow i + 1) = \Delta\Phi_{\%}(i \rightarrow i +$
 288 $1, 100\%)$.

289 *2.4. Uncertainty in the integrated flux estimations*

290 *2.4.1. Uncertainty propagation model*

291 As the instantaneous SSC and discharge values are obtained separately,
292 the relative variance of the instantaneous SSF can be expressed as the sum
293 of the relative variances σ_Q^2 and σ_{SSC}^2 of these variables:

$$\sigma_\phi = \sqrt{\sigma_Q^2 + \sigma_{SSC}^2} \quad (6)$$

294 According to the methodology developed in the GUM (Joint Committee
295 for Guides in Metrology, 2008), the same decomposition of each relative
296 variance σ_Q and σ_{SSC} is performed to take into account all significant sources
297 of uncertainty. In the proposed error propagation model, σ_Q and σ_{SSC} are
298 assumed time-averaged.

299 *2.4.2. Uncertainty of the discharge values*

300 Uncertainties in the discharge values of the data set come mainly from
301 three sources: the measurement method ($\sigma_{Q,Meas}$), the numerical model
302 ($\sigma_{Q,Mod}$) and, eventually the temporal linear interpolation ($\sigma_{Q,Int}$).

$$\sigma_Q = \sqrt{\sigma_{Q,Meas}^2 + \sigma_{Q,Mod}^2 + \sigma_{Q,Int}^2} \quad (7)$$

303 *Measurement method ($\sigma_{Q,Meas}$).* The same measurement method is used at
304 the four measurement sites where discharge values are available. These mea-
305 surements are performed using the velocity-area method, which consists in
306 sampling flow velocity and depth across the cross-section for the discrete
307 integration of the discharge. Using these isolated measurements, a rating
308 curve is extrapolated to transform the continuously measured water levels
309 into discharge values. The uncertainties resulting from this method are en-
310 tirely site dependant. Le Coz et al. (2012) proposed a method to estimate
311 the uncertainty of this measurement method at site A2 during dam flushing
312 in 2011. Using these results, the value $\sigma_{Q,Meas} = 7\%$ was chosen. It is of
313 the same order of magnitude of the uncertainty estimated by Olivier et al.
314 (2008) from well documented rating curves of several mountainous discharge
315 stations.

316 *Numerical modelling ($\sigma_{Q,Mod}$).* For each flushing event, the simulated instan-
317 tantaneous discharges were compared to those observed on the four measurement
318 sites. The time transfer of the water wave is well reproduced by the model for

319 each flushing, as are the maximum discharge values. The standard deviation
 320 between the measured and modelled discharge was estimated systematically
 321 using the following equation:

$$\sigma_{Mi} = \frac{1}{N} \sum_{j=1}^N \left| \frac{Q_{mod}(j) - Q_{meas}(j)}{Q_{meas}(j)} \right| \quad (8)$$

322 The σ_{Mi} -values vary from 2% to 7% with an averaged value around 5%.
 323 Larger values correspond generally to low flow discharges, which are not as
 324 accurately modelled. However, these low flow discharges are not significant
 325 in term of overall fluxes.

326 *Effect of temporal sampling frequency ($\sigma_{Q,Int}$).* Water levels are measured
 327 continuously or calculated numerically with a small time step, so the tem-
 328 poral effect of the linear interpolation (used to compute the instantaneous
 329 suspended sediment flux at every time step) is neglected for the discharge
 330 values. As this assumption is not correct for the SSC measurements, this
 331 source of uncertainty is taken into account in the following part.

332 2.4.3. Uncertainty of the SSC values

333 Four main sources of uncertainty are identified concerning the SSC values:
 334 the vertical ($\sigma_{SSC,VH}$) and transversal heterogeneity ($\sigma_{SSC,HH}$) of the SSC
 335 in a river cross-section, the different measurement methods used (sampled-
 336 filtered-wetted ($\sigma_{SSC,Spl}$), or from turbidity measurement ($\sigma_{SSC,Tu}$)) and the
 337 effect of linear interpolation ($\sigma_{SSC,Int}$).

$$\sigma_{SSC} = \sqrt{\sigma_{SSC,HH}^2 + \sigma_{SSC,VH}^2 + \sigma_{SSC,Spl}^2 + \sigma_{SSC,Tu}^2 + \sigma_{SSC,Int}^2} \quad (9)$$

338 *Spatial heterogeneity ($\sigma_{SSC,HH}$ and $\sigma_{SSC,VH}$).* SSC values are measured as-
 339 suming a homogeneity throughout river cross-section. Vertical homogeneity
 340 depends on the degree of turbulence of the river flow, the grain size distri-
 341 bution of the suspended sediments and the geometry of the river bed. Some
 342 studies (Ryan and Boufadel, 2006; Horowitz et al., 1990) have shown that the
 343 homogeneity of suspended sediment is highly site dependant. Vertical SSC
 344 distribution has never been estimated on the Arc and Isère Rivers, because of
 345 the high flow velocities during flushing events. However, the Rouse-Schmidt
 346 number $Z = W_s/(\kappa u_*)$ (with W_s : settling velocity of the suspended sed-
 347 iments, $\kappa = 0.41$: Von Karman constant, and u_* : friction velocity) gives

348 information on the potential vertical heterogeneity of the suspension (Gar-
349 cia, 2008). Very low values of the Rouse-Schmidt number ($Z \ll 1$) indicate
350 that the suspended sediments are well distributed over the vertical dimen-
351 sion of the river cross-section. Such vertical homogeneity was also verified
352 on a secondary channel of the Arc River (Camenen et al., 2018). Antoine
353 et al. (2012) measured the settling velocity of suspended sediments during
354 the flushing event of 2011 and observed a maximum value $W_s = 2$ mm/s.
355 Using the numerical hydraulic model to estimate u_* , the maximum value of
356 the Rouse-Schmidt number calculated is thus $Z = 3 \times 10^{-2}$, which yields
357 theoretically a relative standard deviation of 3% from the mean value on the
358 SSC profile. As a consequence, we assume hereafter that $\sigma_{SSC,VH} = 3\%$. It
359 should be noted that this value would be higher while including the sand
360 fraction.

361 Lateral homogeneity is mainly function on the lateral variability in tur-
362 bulence, and so on the lateral variability in bed roughness. It was studied
363 during the flushing of 2006 (Némery et al., 2013) on the Isère River at site I1,
364 where the river slope is the mildest (0.1 %) and the river cross-section is the
365 widest (100 meters). The measurements were performed at three sampling
366 positions at the surface (left, middle and right side of the section). The av-
367 erage value of the standard deviation was $\sigma_{SSC,HH} = 5\%$ between the middle
368 of the section and the left and right sides, and the error occurred mainly
369 during the lowering phase of the flushing event.

370 These two values ($\sigma_{SSC,VH} = 3\%$ and $\sigma_{SSC,HH} = 5\%$) are used at every
371 measurement site, for every flushing event. These uncertainty values may be
372 locally higher near confluences. Indeed, in case of a confluence, the lateral
373 homogeneity also depends on the longitudinal mixing and the distance to
374 the confluence. However, since all measurement sites are far enough from
375 confluences (except A2, which has been skipped), this local effect is neglected.

376 *Measurement method* ($\sigma_{SSC,Spl}$ and $\sigma_{SSC,Tu}$). The SSC measurement method
377 plays a key role in error production. For this study, two different methods
378 were used to measure the SSC: a direct method, using automatic or manual
379 samples, and an indirect method, using a turbidimeter.

380 The error produced by the first method was studied in laboratory (Mano,
381 2008). The repeatability of the measurement was tested 40 times on sev-
382 eral samples, over a range of SSCs from 0.02 to 1 g/l. This experimental
383 study showed that the relative standard deviation decreased rapidly with
384 SSCs from 20.1% to 5.5%. Another experiment was performed with higher

385 concentrations (about 10 g/l), and confirmed the decrease of the mean stan-
 386 dard deviation to 2.5%. Since most of the measured concentrations during
 387 a flushing event vary from 1 to 30 g/l, the relative standard deviation from
 388 the direct sampling method was assumed equal to $\sigma_{SSC,Spl} = 2.5\%$.

389 Navratil et al. (2011) gave a global uncertainty value resulting from the
 390 turbidimeter sampling method. The authors estimated a relative standard
 391 deviation of 5% at high concentrations (more than 10 g/l) and 10% at lower
 392 concentrations (between 1 and 10 g/l). In the data set presented in Table 1,
 393 most of the SSC values obtained from a turbidimeter were lower than 10 g/l.
 394 Thus the relative standard deviation is fixed at $\sigma_{SSC,Tu} = 10\%$. However, for
 395 the specific cases of flushing event, turbidity measurements were generally
 396 combined with regular ISCO sampling; as a consequence, we reduced the
 397 error to 5%.

398 *Effect of temporal sampling frequency ($\sigma_{SSC,Int}$).* The term $\sigma_{SSC,Int}$ has to be
 399 estimated due to the heterogeneity of the sampling frequencies for the SSC
 400 measurements. A simple formula is proposed to estimate this term: between
 401 two measured SSC values SSC_i and SSC_{i+1} separated by the time inter-
 402 val Δt , the local relative error could be estimated as the product $|SSC_i -$
 403 $SSC_{i+1}| \times \Delta t$, normalized by the averaged SSC value $(SSC_i + SSC_{i+1})/2$
 404 and the time period T_{event} of the flushing event. Finally, the relative stan-
 405 dard deviation resulting from the interpolation can be expressed for a whole
 406 instantaneous SSC signal of N values as:

$$\sigma_{SSC,Int} = \frac{1}{N} \sum_{i=1}^N \frac{|SSC_i - SSC_{i+1}| \times \Delta t}{T_{event} \times \frac{SSC_i + SSC_{i+1}}{2}} \quad (10)$$

407 As observed in Figure 3, $\sigma_{SSC,Int}$ decreases with the number of sampled
 408 SSCs during the event. This result allows defining a sampling strategy during
 409 the flushing event. This indicator varies from about 0.004% for a very high
 410 frequency signal (turbidimeter) to 24% for a low frequency signal (manual
 411 sampling with a frequency lower than one sample per hour). Whatever the
 412 case, uncertainties due to sampling frequency become negligible as soon as
 413 there is at least one sample every 30 mn ($\sigma_{SSC,Int} \approx 3\%$). The high frequency
 414 obtained thanks to turbidimeters is therefore not so beneficial in terms of
 415 overall uncertainty since $\sigma_{SSC,Tu} = 10\%$.

416 2.5. Significance of the local mass balance

417 Knowing the uncertainty in the integrated flux estimations, the signifi-

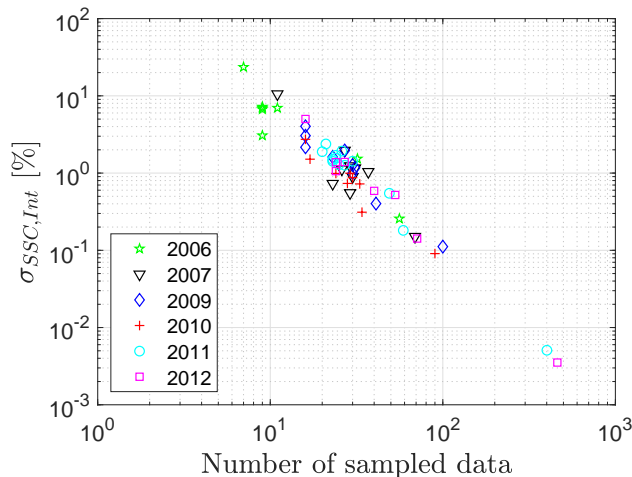


Figure 3: Interpolation error for the SSC as a function of the number of sampled data.

418 cance of the local mass balance $\Delta\Phi(i \rightarrow i + 1)$ can be evaluated regarding
 419 the confidence interval of the integrated fluxes calculated at two consecutive
 420 measurement sites. The condition for a significant erosion or deposition rate
 421 between two consecutive measurement sites is thus the following :

$$|\Phi(X_{i+1}) - \Phi(X_i)| > \sigma_{\Phi}(X_{i+1}) + \sigma_{\Phi}(X_i) \quad (11)$$

422

423 3. Results

424 3.1. Total fluxes and global uncertainty

425 The calculated values of $\Phi(X_i)$ and their associated relative uncertainties
 426 σ_{Φ} are presented in the Table 2. Measurements were not achieved every year
 427 at the 14 sites generally due to experimental difficulties.

428 The uncertainty values of the integrated fluxes vary between 9.2% and
 429 25.9%, with a mean and median values of 11.5% and 10.7% respectively. Fig-
 430 ure 4 shows an example of the global uncertainty profile for the 2010 dam
 431 flush, with the SSC, discharge and global uncertainty profiles (Figure 4a),
 432 and the resulting confidence interval $\Phi(X_i) \pm \sigma_{\Phi}(X_i)$ (Figure 4b). The global
 433 uncertainty stems in almost equal proportions from the uncertainties on dis-
 434 charge and SSC. The results are similar for the other flushing events, except
 435 for the case of very scattered SSC samples. In these cases the contribution
 436 of the SSC uncertainties is predominant (e.g. in 2006).

Table 2: Summary of the global uncertainty σ_Φ (in %) associated with the flux Φ at the 14 sites (in 10^3 Tons).

Site	2006		2007		2009		2010		2011		2012	
	Φ	σ_Φ										
A10	-	-	11.7	13.1	20.1	10.9	29.1	10.2	14.5	11.0	51.6	12.3
A9	39.5	13.4	16.5	13.2	-	-	-	-	-	-	-	-
A8	36.6	13.3	21.3	13.1	24.9	11.2	36.3	10.3	18.0	11.1	-	-
A7	44.4	13.1	22.2	13.1	16.9	12.6	25.2	12.6	14.7	12.6	57.5	12.6
A6	63.6	26.1	23.6	13.1	20.3	11.0	32.2	10.7	19.2	11.4	-	-
A5	39.1	11.1	18.5	9.9	21.7	9.9	33.6	9.8	19.5	9.9	48.4	9.9
A4	-	-	21.8	12.7	17.5	12.5	31.9	11.0	19.2	13.0	53.3	10.3
A3	39.0	13.8	24.9	12.3	17.4	12.3	33.8	10.8	21.3	12.9	71.9	10.7
A1	-	-	38.7	15.8	16.9	12.2	33.0	10.5	28.8	14.5	65.6	10.4
I4	-	-	-	-	15.8	12.1	-	-	-	-	-	-
I3	-	-	-	-	-	-	33.1	12.7	17.5	12.6	79.6	9.8
I2	40.9	12.9	-	-	-	-	52.9	10.3	17.9	11.0	-	-
I1	56.6	13.5	42.0	12.6	20.2	12.6	46.6	12.6	19.7	12.6	68.1	12.8

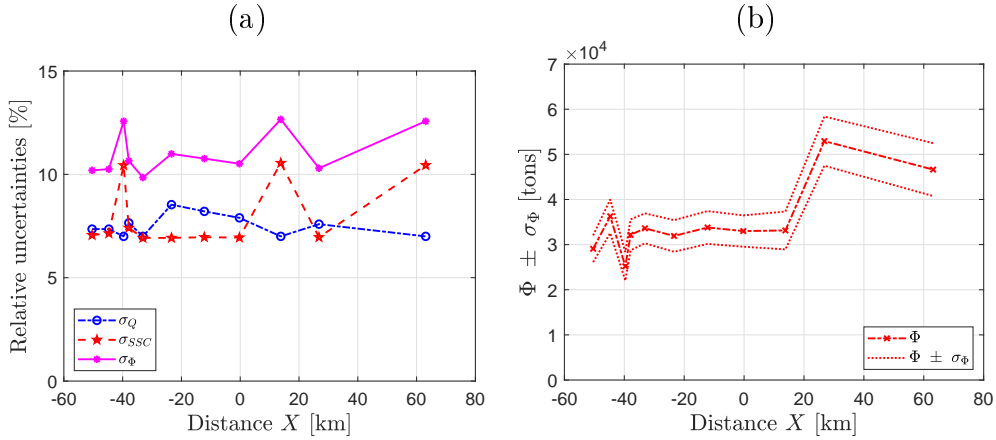


Figure 4: Spatial variation of the uncertainties in fine sediment concentration, discharge, and fine sediment flux estimations for the 2010 dam flushing event (a) and confidence interval resulting from the estimation of global uncertainties (b).

437 *3.2. Spatial evolution of total fluxes*

438 As the first measurement site A10 is located only one kilometre down-
 439 stream to the SMLP dam, it gives the mass output from the three Arc River

440 dams. In Figure 5, we can see that this total input of sediment from dams varied
 441 from 12,000 tons in 2007 to 40,000 tons in 2006 (at A9) and 52,000 tons in
 442 2012 . These variations in the storage and removal of fine sediment from the
 443 reservoirs depend on the upstream watershed incomes and dam management
 444 operations during the year separating two consecutive flushing events. It
 445 should be noted that in Figure 5, a decrease (respectively increase) in $\Phi(X_i)$
 446 indicates deposition (respectively erosion). For the 2012 flushing event, a
 447 larger erosion was observed due to the much larger discharge during the first
 448 step of the flushing event that led to a much significant erosion of the dam
 449 reservoirs.

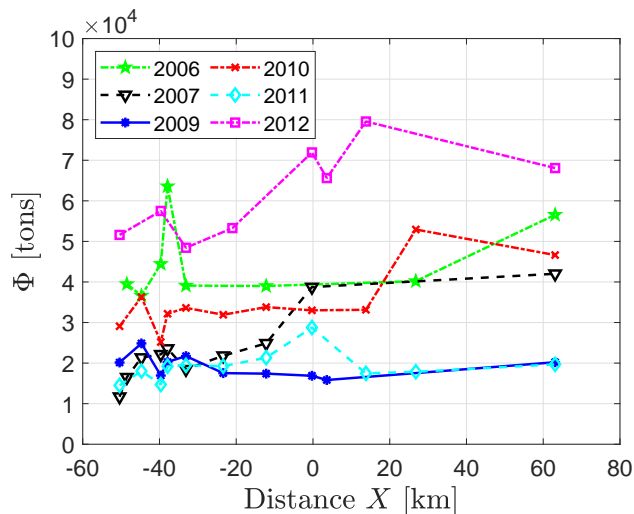


Figure 5: Spatial profiles of the integrated suspended sediment fluxes $\Phi(X_i)$.

450 Over the whole river system, the values of $\Phi(X_i)$ vary widely depending
 451 on the flushing event with some clear difference on the Arc and Isère rivers,
 452 respectively:

- 453 - On the Arc River, between A10 (-50 km) and A1 (0 km), $\Phi(X_i)$ was
 454 conserved in 2006, 2009, and 2010, whereas it increased between these
 455 two measurement sites by almost 12,000 tons in 2011 ($\approx +60\%$), and
 456 20,000 tons in 2007 and 2012 ($\approx +50\%$ and $+40\%$, respectively), indi-
 457 cating a large and significant erosion regarding the confidence interval,
 458 especially in the downstream part of the Arc River.

- 459 - On the Isère River, between A1 (0 km) and I1 (63 km), $\Phi(X_i)$ did not
 460 vary significantly in 2007, 2009; it increased by more than 10,000 tons
 461 in 2006 and 2010 ($\approx +40\%$). In 2011 and 2012, some variations were
 462 observed but on the upstram Isère reach only.
- 463 - Eventually, apart from the 2009 and 2011 events corresponding to the
 464 lowest total fluxes, one can observe a net erosion over the whole river
 465 system from approximately 10,000 tons in 2006 and 2012 to 20,000 tons
 466 in 2007 ($\approx +30\%$, $+40\%$, and $+50\%$, respectively).

467 This indicates that the river bed responds differently to very similar flushing
 468 hydrographs depending on the year. A more detailed analysis of the Φ spatial
 469 evolution shows that even if the value $\Phi(X_i)$ remained the same, conserved
 470 or increased along the entire studied area, specific local variations may occur
 471 especially around St-Jean-de-Maurienne ($X \approx -40$ km) and in the Isère
 472 River straight after the confluence with the Arc River ($0 < X < 15$ km).
 473 Strong positive or negative gradients of $\Phi(X_i)$ can be observed, which indicate
 474 potentially strong local deposition or erosion processes.

475 3.3. Local mass balance

476 Regarding the confidence interval, some local variations of $\Phi(X_i)$ appear
 477 to be not significant. As an example, the magnitude of the local variations
 478 observed between A4 ($X = -24$ km), A5 ($X = -33$ km) and A6 ($X =$
 479 -38 km) is not high enough to be significant regarding the confidence interval
 480 for most flushing events. Fig. 4b shows on the opposite a strong positive
 481 variation between I3 ($X = 14$ km) and I2 ($X = 27$ km) in 2010, which is
 482 significant regarding the confidence interval.

483 Table 3 presents the values of the local mass balance $\Delta\Phi(i \rightarrow i + 1)$
 484 (expressed in 10^3 tons) along the study area. If $\Delta\Phi(i \rightarrow i + 1) > 0$, this
 485 means that resuspension occurs between two consecutive measurement sites
 486 located at positions X_i and X_{i+1} . If $\Delta\Phi(i \rightarrow i + 1) < 0$, this means that
 487 deposition occurs between the two consecutive measurement sites. The local
 488 mass balance values which are confirmed by the confidence intervals are given
 489 in bold font in Table 3 following Eq. 11. It should be noted that depending on
 490 the year, some intervals have been aggregated due to the absence of data in
 491 some sites. It does not affect the results since the condition proposed (Eq. 11)
 492 does not depend on the distance between the two consecutive measurement
 493 sites.

Table 3: Local mass balance ($\Delta\Phi(i \rightarrow i + 1)$, in 10^3 tons) distribution in the Arc-Isère river system for the six studied dam flushing events (bold values correspond to significant values regarding the global uncertainty value, positive values correspond to erosion whereas negative values correspond to deposition).

Reach	2006	2007	2009	2010	2011	2012
A9-A10	–	+4.8	+4.7	+7.2	+3.5	+5.9
A8-A9	–2.9	+4.8				
A7-A8	+7.8	+0.8				
A6-A7	+19.1	+1.4	+3.3	+7.0	+4.5	–9.1
A5-A6	–24.5	–5.1	+1.5	+1.4	+0.2	
A4-A5	–0.1	+3.3	–4.2	–1.7	–0.2	+4.8
A3-A4		+3.1	–0.1	+1.9	+2.1	+18.7
A2-A3	+1.2	+13.9	–0.5	–0.8	+7.4	–6.3
A1-A2		+3.3	–1.0	+0.1	–11.3	+14.0
I4-A1						
I3-I4			–6.3	+1.8		
I2-I3	+16.4	–11.5				
I1-I2						

494 Table 3 indicates that only 14 of the 52 local mass balances are signifi-
495 cant for the proposed uncertainty model propagation: 5 of the 19 negative
496 mass balances, and 9 of the 33 positive mass balances. However, significant
497 local mass balances highlight different behaviours of the river bed evolu-
498 tion: in 2010, a significant deposition is observed just upstream a strong
499 re-suspension, even if the two successive river reaches (separating A8, A7
500 and A6) have almost the same mean slopes (about 1%) and reach lengths
501 are smaller than 5 kilometres. More generally, we can see that flushing events
502 produce significant dynamics in terms of exchange with the river bed, with
503 values of re-suspension or deposition of fine sediments up to 20,000 tons .

504 Despite this relatively low significance of the local mass balance values,
505 meaningful tendencies may explain why local variations can be significant for
506 one flushing event but not significant for the next one. More generally, the
507 responses of the river bed can be divided into two groups: the river bed gave
508 similar responses for 2009, 2010 and 2011 (group 1), and similar responses for
509 2006 and 2007 (group 2). The difference observed between the mass balance
510 distributions of groups 1 and 2 is particularly evident for upstream sites in

511 the Arc River, where the slope of the river bed is high: for example, high
512 erosion of the bed was observed between measurement sites A8 and A7 before
513 the year 2008, whereas systematic deposition was observed after this year.
514 The same behaviour was observed between sites A5 and A4, whereas the
515 opposite was observed between sites A6 and A5. The two groups of flushing
516 events were separated by a major event: in May 2008 a natural flood flowed
517 from the upper Arc catchment (15-year return period). Regarding previous
518 results, the bed changes due to this flood significantly modified the local mass
519 balance distribution. Jaballah et al. (2015) showed evidences on these large
520 effect of the 2008 flood on the river morphology on a 5 km long reach (located
521 between A6 and A5), which confirms its impact on SSF dynamics. The flood
522 that occurred in May 2010 (the second highest in intensity during the study
523 period), and which affected in similar proportions all the sub-catchments of
524 the Isère watershed, did not change this local mass balance distribution. The
525 difference of behaviour between flushes could also be partly explained by the
526 settling properties of sediments that can change depending on the storage
527 duration in dam reservoirs (Legout et al., 2018). Indeed, most deposits in
528 dam reservoirs form during the spring period. Depending on the exact date
529 of the dam flushing, their storage duration can vary from a few days to a few
530 months depending on the hydrology.

531 4. Discussion

532 4.1. Spatio-temporal dynamics of discharge and SSC

533 The analysis of SSC and discharge signals gives information on their vari-
534 ability along both rivers and could provide some clues about the differences
535 in flux dynamics from one flushing event to another. In Figure 6, the dis-
536 charge and concentration measurement are presented for the dam flushes of
537 2007 and 2009 at Pontamafrey (A7) and Grenoble (I1), respectively.

538 On site A7, the SSC patterns resulting from the 2007 and 2009 flushing
539 events differ in shape and magnitude. In 2007 the peak SSC value (16.7 g/l)
540 was measured during the first discharge step of the flushing hydrograph,
541 whereas the peak value of the 2009 SSC signal (10.9 g/l) appeared during the
542 second discharge step. These differences may be explained by the availability
543 of the fine sediments and the erosion processes in the three dam reservoirs of
544 the Arc River. In 2007, the SSC peak value corresponds to sediments that are
545 easily removed from the reservoirs, while the second part of the SSC signal
546 is related to sediments removed due to higher bed shear stresses (higher

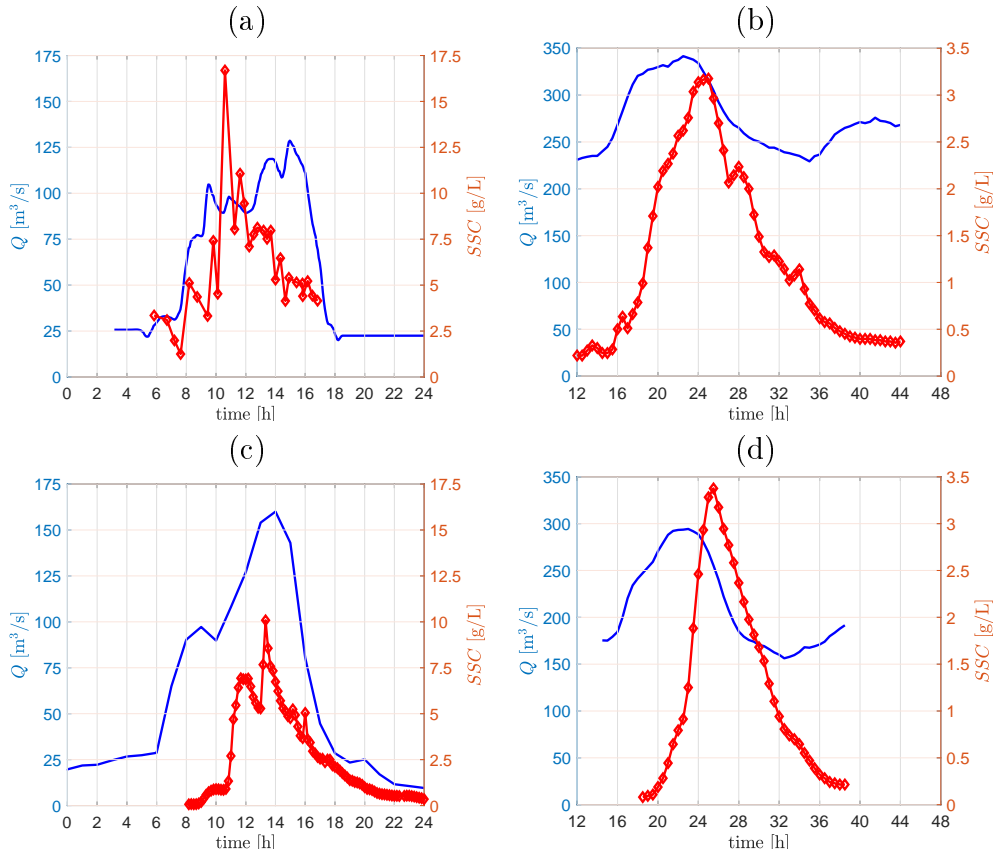


Figure 6: Water discharge and concentration time-series at sites A7 (Pontamafrey, a and c) and I1 (Grenoble, b and d) for the 2007 (a and b) and 2009 (c and d) flushing events.

547 discharge values, super-critical flows in the dam reservoirs). In 2009 the
 548 sediments of the dam reservoirs were more difficult to remove, and the SSC
 549 signal increased only from the increasing part of the second discharge step.
 550 As a consequence, the sediment input is highly function of the hydrology
 551 during the months preceding the flushing event, and so the accumulation of
 552 fresh fine sediments in dam reservoirs during the spring period. On site I1,
 553 the SSC signals are smoothed, because of the long distance travelled along
 554 the river and the dispersion processes; the differences between the SSC peak
 555 values are attenuated. One should note that the SSC peak is measured
 556 systematically after the discharge peak of the hydrograph since the flood
 557 wave travels faster than flow velocity.

558 *4.2. Hydrology influence on SSC dynamics*

559 In order to understand the possible influence of the hydrology on the
 560 fine sediment dynamics, we define an average discharge for the spring season
 561 before the flushing event $Q_{m,spring}$ (i.e. from the 1st April to the day before
 562 the flushing event) at both A7 and I1 location, as well as a base discharge
 563 $Q_{m,base}$ during the flushing event on the Isère River at I1 location (averaged
 564 discharge on the day before the flushing event). Indeed, the Q_{max} values are
 565 almost the same whatever the event on the Arc River; they increase only with
 566 the input from tributaries, i.e. at the Isère restitution ($X = -8$ km), the
 567 Isère confluence ($X = 0$ km), and at the Cheylas restitution ($X = +20$ km).
 568 Results are presented in Tab. 4 together with the concentration peak values
 569 measured at A7 location for both discharge step.

Table 4: Mean discharges at Pontamafrey (A7) and Grenoble (I1) during the spring period before flushing events ($Q_{m,spring}$) and at the restitution near A2 site ($Q_{m,rest}$), peak concentrations for the first (C_{p1}) and second (C_{p2}) plateau of the event, and cumulative SSF ($\Phi_{tot,spring}$) measured at site I1 during the 3 months preceding each flushing event.

Site	A7			A2	I1		
Year	$Q_{m,spring}$ m ³ /s	C_{p1} g/l	C_{p2} g/l	$Q_{m,rest}$ m ³ /s	$Q_{m,spring}$ m ³ /s	$Q_{m,base}$ m ³ /s	$\Phi_{tot,spring}$ 10 ³ tons
2006	30.0	9	24	83	246	229	950
2007	33.5	17	8	56	208	232	400
2009	36.0	1	10	52	210	201	430
2010	35.5	3	12	98	209	368	1,000
2011	33.5	5	13	33	116	165	125
2012	27.0	12*	42	55	261	444	650

*: a third intermediate peak concentration at 20 g/L was observed because of the unexpected peak discharge in the middle of the first plateau.

570 In general, the second peak of concentration during the 2nd plateau is
 571 higher than the first one since bed shear stresses are higher in the dam
 572 reservoirs. However, in 2007, a lower value is observed indicating a smaller
 573 stock of fine sediments in the reservoirs. It could be explained by the flood
 574 event in September 2006 ($Q_{max} \approx 150$ m³/s). Only two other significant
 575 floods, for which dam gates were opened, were observed during the period
 576 between 2005 and 2012: the May 2008 flood ($Q_{max} \approx 450$ m³/s) and the
 577 June 2010 flood ($Q_{max} \approx 160$ m³/s). Similarly, the following flushing event

578 in 2009 and 2011 yielded a low total flux Φ just after dam reservoirs, i.e.
579 $\Phi < 20,000$ tons. The initial total flux from dam reservoir is thus function
580 of the duration without dam operation. On the other hand, the hydrology
581 during the spring period does not appear to influence significantly the amount
582 of fine sediment to be eroded. No correlation could be found between the
583 average flow $Q_{m,spring}$ on the two month prior to the flushing event and the
584 initial total flux.

585 Also, we note that erosion generally occurred in the Isère River when the
586 base discharge $Q_{m,base}$ in the Isère River is the highest (2006, 2010, and 2012).
587 This could be explained as the gravel bar were then flooded and fine sediment
588 stocks over gravel bars could be resuspended. However, for the 2012 event,
589 which reached the largest discharges (close to $500 \text{ m}^3/\text{s}$), highest vegetated
590 part of gravels bars have been flooded and have enhanced deposition. We
591 expect to relate erosion on the downstream part of the Arc River observed
592 in 2007, 2011, and 2012 with the additional flow discharge coming from the
593 restitution ($Q_{m,rest}$). However, no clear correlation could be made.

594 *4.3. Initial quantity of erodible sediments in the river bed*

595 Continuous SSF measurements at site I1, which integrate the whole study
596 area, are available over the whole period of the study (with a sampling step
597 of 30 minutes). More specifically, the cumulative SSF measured at site I1
598 during the 2-3 months preceding each flushing (from 1st April) event showed
599 large variations as a function of the event (Tab. 4): from 125,000 tons in
600 2011 to 1,000,000 tons in 2010. The large amounts of sediment mass in
601 2006 and 2010 were mostly due to a very active spring period but also due to
602 some engineering works on the Isère dikes in 2010. Also, a large compensation
603 reservoir directly connected to the Arc River just upstream A7 ($X = -40 \text{ km}$)
604 was cleaned out over a three month period in 2010 and 2011. In 2006 and
605 2010, the 2-month integrated SSF at I1 reached very large values that have
606 potentially led to large deposition over gravel bars. Significant re-suspension
607 have been observed on the Isère River during the flushing events performed
608 these two years, and on the Arc River during the 2006 event, which appears
609 consistent with the hydrology during the spring period. The cleaning of the
610 compensation reservoir in 2011 could also explain the large re-suspension
611 observed in the Arc River during the following flushing event, just upstream
612 the confluence with the Isère River.

613 In any case, the sediment mass transported during a flushing event does
614 not represent more than 5% of the annual suspended sediment mass transiting

615 at site I1. These results corroborate previous estimations of the contribution
616 of hydraulic flushes to annual SSF of the Isère River (Némery et al., 2013).

617 Our results confirm the importance of the suspended sediment dynamics
618 before the event (during the spring period). Indeed, the spatial distribution
619 of sediment deposits strongly affects the possible resuspension of sediment
620 during the flushing event. Some studies (Droppo et al., 2001) have shown
621 the effect of sequential bed depositions under several flow conditions in the
622 bed erosion process, especially if the proportion of cohesive sediments in the
623 total suspended load is non-negligible.

624 4.4. Dynamic mass balance

625 Table 3 gives spatial information on the local mass balances per river
626 reach. For example, the river bed between the two consecutive measurement
627 sites A4 and A3 was systematically eroded as was the river bed between
628 A3 and A1. Furthermore, the lengths of these two reaches are almost equal
629 (≈ 12 km). However, the values of the dynamic and time-normalized mass
630 balance $\Delta\Phi_{\%}(i \rightarrow i+1, t\%)$ (Eq. 5) on these parts of the river bed show very
631 different mass transport dynamics during the flushing events. In Fig. 7 c and
632 d, the values of $\Delta\Phi_{\%}(A3 \rightarrow A1, t\%)$ and $\Delta\Phi_{\%}(A4 \rightarrow A3, t\%)$, respectively,
633 are plotted as a function of the time made dimensionless with the duration of
634 the event T_{event} . Although the two reaches of the river were globally eroded
635 at the end of the flushing event, the A3-A1 reach endured first some large
636 erosion and then some deposition. This succession of erosion and deposition
637 could be explained by an easily erodible mass of sediment on the river bed
638 that was removed by the first discharge step of the flush hydrograph. During
639 the second discharge step, the water level became high enough to flow on
640 gravel bars implying significant deposition. On the other hand, the A4-
641 A3 reach endured successively considerable deposition and then even larger
642 erosion during the same event (Fig. 7 d). On this reach, two large, easily
643 submersible banks and a small dam reservoir were the only remarkable sites.
644 They could indeed explain the following mass balance dynamics from 2009
645 to 2011 events: before the first discharge step, the reservoir was emptied,
646 removing a small proportion of the fine deposited sediments. This first release
647 generated nevertheless a SSC peak at a relative low discharge value and
648 did not influence the global mass balance value. The first discharge step
649 led to considerable deposition on the easily submersible banks which were
650 eventually easily re-suspended by the second discharge step. Furthermore,
651 the second discharge step involved sufficiently high water levels to remove the

652 upper layer of sediment deposited in the small reservoir. The global mass
 653 balances calculated for all the events were in this case not representative of
 654 the temporal dynamics of this reach, where the exchange processes with the
 655 river bed were significant.

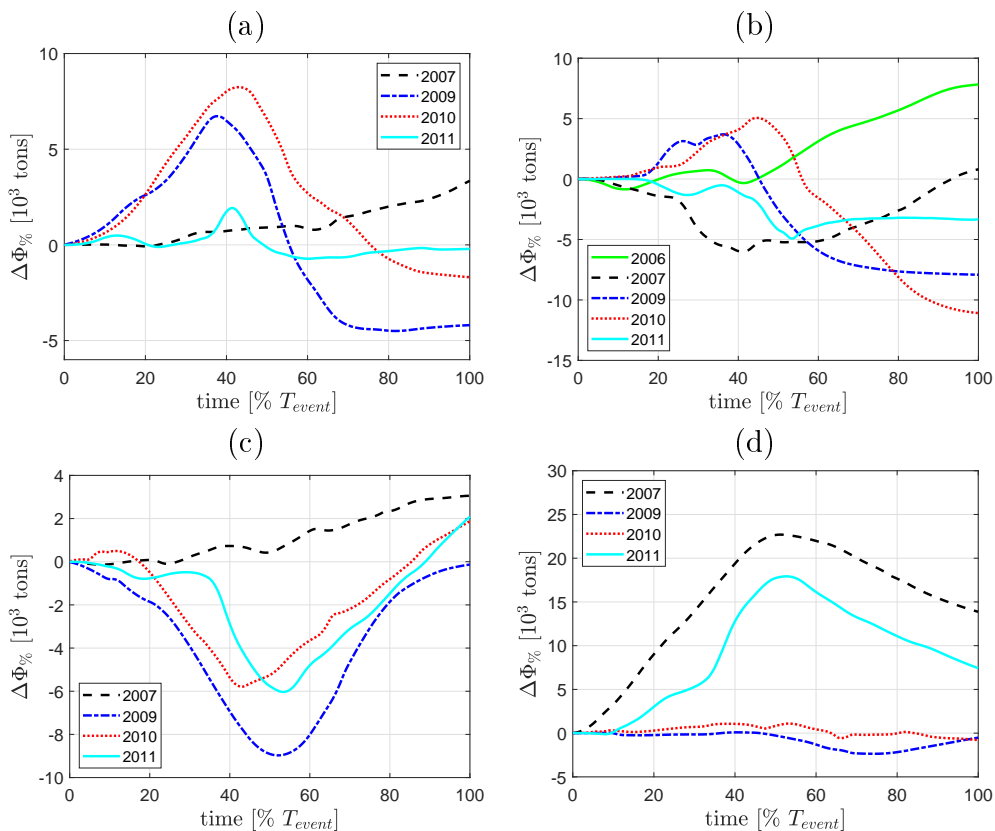


Figure 7: Dynamic cumulative mass balance between A8 and A7 (a), A5 and A4 (b), A4 and A3 (c) and A3 and A1 (d) (a positive value means erosion whereas a negative value means deposition).

656 This cumulative method is also applied to confirm the effect of the flood
 657 in May 2008, as it appears in Table 3 (i.e. different river bed responses
 658 before and after the flood). On the two previous examples from Fig. 7 c
 659 and d, we can see that deposition and erosion dynamics suddenly changed
 660 between 2007 and 2009. Even if the mass balance at the end of the events
 661 remain positive, the dynamics changed from significant exchanges with the
 662 river bed to simple transfer of sediment mass (and vice versa). After 2009,

663 the dynamics tend back to the one observed before the 2008 flood.

664 The dynamic cumulative mass balance for the more upstream reaches
665 A8-A7 and A5-A4 are presented in Fig. 7 a and b, respectively. If the
666 overall impact of the dam flushes on these reaches was generally deposition,
667 they presented a first step of erosion followed by a large deposition on the
668 second part of the event. These two additional examples also confirm the
669 2008 flood impact on SSF dynamics in these two other reaches linked to the
670 large modifications of the river morphology (Jaballah et al., 2015). Indeed,
671 the opposite behaviour was observed in 2007 compared to the events after
672 2008, the global mass balances changing global erosion into global deposition
673 (b) or inverse (a).

674 The four examples presented in Figure 7 show that the river reaches have
675 not the same ability to recover the prior-flood equilibrium : reaches like the
676 ones between A5 and A4 or A3 and A1 show in 2011 very similar dynamics
677 than the one observed in 2007. For the two other reaches, the prior dynamics
678 were still not recovered in 2011. It also shows the dominating influence of
679 river morphology on SSF dynamics.

680 4.5. *Physical characteristics of the transported sediments*

681 Sediments parameters like grain size and/or settling velocity but also
682 suspended concentration are fundamental for predicting deposition processes
683 (Legout et al., 2018). Their variability could also explain observed differences
684 between flushing events or river reaches (Garcia, 2008). In 2011, grain size
685 distribution (GSD) have been measured for every sediment samples at A5,
686 A1 and I1 sites. Grain size characteristics, averaged over the flushing period,
687 are presented in Table 5.

Table 5: Time-averaged values of D_{10} , D_{50} and D_{90} (μm) measured at sites A5, A1 and I1 during the 2011 flushing event.

Site	2011 flushing event		
	D_{10}	D_{50}	D_{90}
A5	3.4	16	51
A1	3.4	17	54
I1	3.1	14	39

688 These grain size measurements show that few differences are observed
689 between the three measurement sites for this event even if a small fining

690 is observed. Only the percentile D_{90} changed significantly between A1 and
691 I1. In 2011, one observed a significant local erosion between A5 and A1
692 and a significant local deposition between A1 and I3 this year. The local
693 deposition between A1 and I3 could be related to the decrease of D_{90} values
694 with a position of the coarsest particles downstream the confluence with the
695 Isère River. During the flushing event of June 2011, the additional discharge
696 coming from the upper Isère River was low, and the flow velocity could have
697 decrease significantly downstream the confluence where the river width is
698 larger.

699 Despite the significant local erosion observed between A5 and A1, no
700 change were measured in terms of grain size distributions. Fig. 7 b, c and
701 d shows the local dynamics of erosion and deposition between A5 and A1.
702 In 2011, the flux was globally transferred between A5 and A4 with a first
703 period of deposition followed by a period of erosion. In this case, one can
704 conclude that the freshly deposited sediments during the first part of the event
705 have been re-suspended during the second part of the event explaining the
706 constant GSD. However, between A3 and A1, the opposite behaviour is ob-
707 served. Previous sediments deposits on the river bed were replaced by the
708 suspended sediments coming from upstream. However, a similar GSD is ob-
709 served indicating a certain consistency of the long term dynamics of the fine
710 deposits in these reaches.

711 5. Conclusion

712 Six field campaigns were analysed to evaluate the impact of dam flushing
713 events on suspended sediment dynamics downstream of the dams. SSC and
714 discharge measurements were performed on the Arc and Isère Rivers, France,
715 at 14 sites in June 2006, 2007, 2009, 2010, 2011, and 2012. These intensive
716 measurement campaigns allowed an estimation of suspended sediment fluxes
717 along the reaches of both rivers as well as the local mass balance.

718 To estimate the significance of the observed local variations, a propagation
719 model for the uncertainty on the global flux was built, taking into account
720 the main sources of error for both SSC and discharges. The mean calculated
721 uncertainty value was $\sigma_{\Phi} = 11.5\%$. These uncertainty values confirm the
722 global tendency of suspended sediment flux propagation, whereas only 14
723 out of 52 local mass balances between two consecutive measurement sites
724 were significant. Also, a dynamic time-normalized method was developed

725 to evaluate and discuss temporal variations of the mass balance during one
726 flushing event.

727 Even if the dam flushing operating protocol was identical over the years
728 (except for 2012), the suspended sediment mass removed from the reservoirs
729 varied from 10,000 tons in 2007 to 40,000 tons in 2006. The hydrology on
730 the Upper Arc River during the previous spring period significantly affected
731 the efficiency of these flushing events. On the other hand, the global fine
732 sediment mass balance along the studied river segment varied from zero in
733 2011 and 2009 to 30,000 tons in 2007 indicating also a strong effect of the
734 initial state: stock of fine sediments in the river but also river geometry.

735 We showed that the bed morphology significantly modified the fine sedi-
736 ments dynamics. Indeed, the May 2008 flood, a 15-year return period flood
737 on the Arc River that largely modified both Arc and Isère river morphologies
738 yielded major changes in fine sediment dynamics during flushing events. In-
739 deed, opposite behaviour were observed for many reaches in terms of global
740 mass balance (after the flushing event) but also in terms of temporal dynam-
741 ics during the event (erosion followed by deposition or the opposite).

742 Another point to be addressed is the quantity and quality of the fine
743 sediment stocks in the river bed, i.e. surface deposits and stocks infiltrated
744 in the bed matrix. Indeed, our knowledge of the stocks remains very limited.
745 It would be important to evaluate the quantity of available sediments as
746 deposits but also stocked in the river bed that could be re-suspended as soon
747 as coarse particles are mobilized (Navratil et al., 2010; Misset et al., 2019).
748 More continuous monitoring of SSF, but also direct measurements on the
749 river bed and in dam reservoirs are necessary to estimate the initial state of
750 the river bed and the availability of the fine sediments in reservoirs.

751 To better predict the effect of dam flushing, investigations must now focus
752 on combining the analysis of local morphodynamics and global hydrological
753 aspects more in detail. It could be eventually made in the future thanks to
754 repeated Lidar surveys, assuming that topographic changes are only due to
755 fine sediment dynamics and only occur on gravel bars. An important issue
756 is the sand fraction. It corresponds indeed to approximately 50% of the
757 deposit volume (Camenen et al., 2016) whereas sand flux are not captured
758 by the turbidimeters nor by the surface sampling network. Also, the use of a
759 numerical model to calculate downstream sediment propagation would help
760 dam operators to optimize dam flushing scenarios.

761 *Acknowledgements*

762 This work has been partially supported by the French National Research
763 Agency (ANR) under the grant ANR-18-CE01-0020 (DEAR project). The
764 study took place on an experimental site of the ZABR (Zone Atelier du Bassin
765 Rhône) which is a CNRS-labelled site. We would like to thank all the persons
766 from INRAE (River hydraulic team of RiverLy, Lyon), IGE (Hydrimz team,
767 Grenoble) and EDF (DTG, Grenoble) who produced all the field data used
768 in this study.

769 **References**

- 770 Alcaiyaga, H. A., Mao, L. C., and Belleudy, P. (2018). Predicting the geo-
771 morphological responses of gravel-bed rivers to flow and sediment source
772 perturbations at the watershed scale: an application in an alpine water-
773 shed. *Earth Surface Processes and Landforms*, 43(4):894–908.
- 774 Antoine, G. (2013). *Dynamique des matériaux en suspension le long de riv-
775 ières aménagées de montagne. Exemple de l’Arc en Maurienne et de l’Isère*
776 *[Suspended sediment dynamics along engineered alpine rivers. Exemple of*
777 *the Arc en Maurienne and Isère rivers]*. PhD thesis, Grenoble University,
778 Grenoble, France. 282 p. (in French).
- 779 Antoine, G., Jodeau, M., Camenen, B., and Esteves, M. (2012). A settling
780 velocity parameterization for sand/mud mixture in a 1d flow during a
781 flushing event. In *Proc. 6th River Flow Conference*.
- 782 Asaeda, T. and Rashid, H. (2012). The impacts of sediment released from
783 dams on downstream sediment bar vegetation. *Journal of Hydrology*, 430-
784 431:25 – 38.
- 785 Bilotta, G., Burnside, N., Cheek, L., Dunbar, M., Grove, M., Harrison,
786 C., Joyce, C., Peacock, C., and Davy-Bowker, J. (2012). Developing
787 environment-specific water quality guidelines for suspended particulate
788 matter. *Water Research*, 46:2324–2332.
- 789 Brandt, S. (1999). Sedimentological and geomorphological effects of reservoir
790 flushing: The Cachi reservoir, Costa Rica, 1996. *Geografiska Annaler A*,
791 81:391–407.

- 792 Brandt, S. (2000). Classification of geomorphological effects downstream of
793 dams. *Catena*, 40:375–401.
- 794 Camenen, B., Dramais, G., Buffet, A., Thollet, F., Le Bescond, C., Lagouy,
795 M., Berni, C., and Le Coz, J. (2018). Estimation of sand suspension in a
796 secondary channel of an alpine river. In Paquier, A., Rivière, N., and Kha-
797 ladi, A., editors, *River Flow, Proc. 9th Int. Conf. on Fluvial Hydraulics*,
798 number 04014 in E3S Web of Conferences 40, pages 1–8, Lyon, France.
- 799 Camenen, B., Herrero, A., Perret, E., Berni, C., Thollet, F., Buffet, A.,
800 Dramais, G., Le Bescond, C., and Lagouy, M. (2016). Estimation of the
801 volume of a fine sediment deposit over a gravel bar during a flushing event.
802 In Constantinescu, G., Garcia, M., and Hanes, D., editors, *River Flow,*
803 *Proc. 8th Int. Conf. on Fluvial Hydraulics*, page 8p., St Louis, Missouri,
804 USA.
- 805 Camenen, B., Jodeau, M., and Jaballah, M. (2013). Estimate of fine sediment
806 deposit dynamics over a gravel bar using photography analysis. *Interna-*
807 *tional Journal of Sediment Research*, 28(2):220 – 233.
- 808 Campisano, A., Creaco, E., and Modica, C. (2004). Experimental and numer-
809 ical analysis of the scouring effects of flushing waves on sediment deposits.
810 *Journal of Hydrology*, 299:324–334.
- 811 Campisano, A., Creaco, E., and Modica, C. (2008). Laboratory investigation
812 on the effects of flushes on cohesive sediment beds. *Urban Water Journal*,
813 5:3–14.
- 814 Chang, H., Harrison, L., Lee, W., and Tu, S. (1996). Numerical modeling
815 for sediment-pass-through reservoirs. *Journal of Hydraulic Engineering*,
816 122:381–388.
- 817 Chung, S. W., Ko, I. H., and Kim, Y. K. (2008). Effect of reservoir flushing on
818 downstream river water quality. *Journal of Environmental Management*,
819 86:139–147.
- 820 Collier, K. J. (2002). Effects of flow regulation and sediment flushing on in-
821 stream habitat and benthic invertebrates in a New Zealand river influenced
822 by a volcanic eruption. *River Research and Applications*, 18:213–226.

- 823 Crosa, G., Castelli, E., Gentili, G., and Espa, P. (2010). Effects of suspended
824 sediments from reservoir flushing on fish and macroinvertebrates in an
825 alpine stream. *Aquatic Sciences*, 72:85–95.
- 826 Dramais, G., Le Coz, J., Camenen, B., and Hauet, A. (2011). Advantages of a
827 mobile LSPIV method for measuring flood discharges and improving stage
828 discharge curves. *Journal of Hydro-environment Research*, 5:301–312.
- 829 Droppo, I., Lau, Y., and Mitchell, C. (2001). The effect of depositional
830 history on contaminated bed sediment stability. *Science of The Total En-
831 vironment*, 266:7–13.
- 832 Espa, P., Batalla, R. J., Brignoli, M. L., Crosa, G., Gentili, G., and Quadroni,
833 S. (2019). Tackling reservoir siltation by controlled sediment flushing:
834 Impact on downstream fauna and related management. *PLoS ONE*, 14(6-
835 e0218822):1–26.
- 836 Espa, P., Crosa, G., Gentili, G., Quadroni, S., and Petts, G. (2015). Down-
837 stream ecological impacts of controlled sediment flushing in an alpine valley
838 river: a case study. *River Research and Applications*.
- 839 Frémion, F., Bordas, F., Mourier, B., Lenain, J.-F., Kestens, T., and Courtin-
840 Nomade, A. (2016). Influence of dams on sediment continuity: A study case
841 of a natural metallic contamination. *Science of The Total Environment*,
842 547:282 – 294.
- 843 Garcia, M. (2008). *Sedimentation engineering: processes, measurements,
844 modeling, and practice*. ASCE.
- 845 Goutal, N. and Maurel, F. (2002). A finite volume solver for 1D shallow-water
846 equations applied to an actual river. *International Journal for Numerical
847 Methods in Fluids*, 38:1–19.
- 848 Horowitz, A. J., Rinella, F. A., Lamothe, P., Miller, T. L., Edwards, T. K.,
849 Roche, R. L., and Rickert, D. A. (1990). Variations in suspended sedi-
850 ment and associated trace element concentrations in selected riverine cross
851 sections. *Environmental Science and Technology*, 24:1313–1320.
- 852 Jaballah, M., Camenen, B., Paquier, A., and Jodeau, M. (2015). Alternate
853 bar development in an alpine river following engineering works. *Advances
854 in Water Resources*, 81:103–113.

- 855 Jansson, M. B. and Erlingsson, U. (2000). Measurement and quantification
856 of a sedimentation budget for a reservoir with regular flushing. *Regulated*
857 *Rivers: Research and Management*, 16:279–306.
- 858 Ji, U., Julien, P., and Park, S. (2011). Sediment flushing at the Nakdong
859 River estuary barrage. *Journal of Hydraulic Engineering*, 137:1522–1535.
- 860 Jodeau, M., Hauet, A., Paquier, A., Le Coz, J., and Dramais, G. (2008). Ap-
861 plication and evaluation of LS-PIV technique for the monitoring of river
862 surface velocities in high flow conditions. *Flow Measurement and Instru-*
863 *mentation*, 19:117–127.
- 864 Joint Committee for Guides in Metrology, editor (2008). *Evaluation of mea-*
865 *surement data - Guide to the expression of uncertainty in measurement*
866 *(1995). In his French and revisited version: évaluation des données de*
867 *mesure - Guide pour l'expression de l'incertitude de mesure*. GUM.
- 868 Jourdain, C., Belleudy, P., Tal, M., and Malavoi, J. R. (2017). The role of
869 hydrology on vegetation removal in a heavily managed gravel bed river:
870 the Isère, Combe de Savoie, France. *Geomorphologie: Relief Processus*
871 *Environnement*, 23(3):203–217.
- 872 Khosronejad, A., Rennie, C., Neyshabouri, A. S., and Gholami, I. (2008).
873 Three-dimensional numerical modeling of reservoir sediment release. *Jour-*
874 *nal of Hydraulic Research*, 46:209–223.
- 875 Kondolf, G. M., Gao, Y., Annandale, G. W., Morris, G. L., Jiang, E., Zhang,
876 J., Cao, Y., Carling, P., Fu, K., Guo, Q., Hotchkiss, R., Peteuil, C., Sumi,
877 T., Wang, H.-W., Wang, Z., Wei, Z., Wu, B., Wu, C., and Yang, C. T.
878 (2014). Sustainable sediment management in reservoirs and regulated
879 rivers: Experiences from five continents. *Earth's Future*, 2(5):256–280.
- 880 Kondolf, G. M. and Wilcock, P. R. (1996). The flushing flow problem: Defin-
881 ing and evaluating objectives. *Water Resources Research*, 32:2589–2599.
- 882 Lai, J.-S. and Shen, H. W. (1996). Flushing sediment through reservoirs.
883 *Journal of Hydraulic Research*, 34:237–255.
- 884 Le Coz, J., Camenen, B., Peyrard, X., and Dramais, G. (2012). Uncertainty
885 in open-channel discharges measured with the velocity area method. *Flow*
886 *Measurement and Instrumentation*, 26:18–29.

- 887 Legout, C., Droppo, I. G., Coutaz, J., Bel, C., and Jodeau, M. (2018). As-
888 sessment of erosion and settling properties of fine sediments stored in cob-
889 ble bed rivers: the Arc and Isère alpine rivers before and after reservoir
890 flushing. *Earth Surface Processes and Landforms*, 43(6):1295–1309.
- 891 Liu, J., Minami, S., Otsuki, H., Liu, B., and Ashida, K. (2004). Environ-
892 mental impacts of coordinated sediment flushing. *Journal of Hydraulic*
893 *Research*, 42:461–472.
- 894 López-Tarazón, J. A., Batalla, R. J., Vericat, D., and Francke, T. (2012).
895 The sediment budget of a highly dynamic mesoscale catchment: The River
896 Isábena. *Geomorphology*, 138:15–28.
- 897 Mahmood, K. (1987). Reservoir sedimentation: Impact, extent, and mitiga-
898 tion. Technical report, World Bank, Washington, DC.
- 899 Mano, V. (2008). *Processus conditionnant les apports de sédiments fins dans*
900 *les retenues - Optimisation des méthodes de mesure et modélisation statis-*
901 *tique [Fine sediment supply processes in dam reservoirs: statistic modelling*
902 *and optimization of measurement method]*. PhD thesis, Joseph Fourier
903 University, Grenoble, France. (in French).
- 904 Marnezy, A. (1999). *L’ Arc et sa vallée: Anthropisation et géodynamique*
905 *d’ une rivière alpine dans son bassin versant [The Arc River system: an-*
906 *thropisation and geodynamic of an alpine river system]*. PhD thesis, Joseph
907 Fourier University, Grenoble, France.
- 908 Misset, C., Recking, A., Legout, C., Poirel, A., Cazihlac, M., Esteves, M.,
909 and Bertrand, M. (2019). An attempt to link suspended load hysteresis
910 patterns and sediment sources configuration in alpine catchments. *Journal*
911 *of Hydrology*. (submitted).
- 912 Murle, U., Ortlepp, J., and Zahner, M. (2003). Effects of experimental flood-
913 ing on riverine morphology, structure and riparian vegetation: The river
914 spol, swiss national park. *Aquatic Sciences*, 65:191–198.
- 915 Navratil, O., Esteves, M., Legout, C., Gratiot, N., Nemery, J., Willmore, S.,
916 and Grangeon, T. (2011). Global uncertainty analysis of suspended sed-
917 iment monitoring using turbidimeter in a small mountainous river catch-
918 ment. *Journal of Hydrology*, 398:246–259.

- 919 Navratil, O., Legout, C., Gateuille, D., Esteves, M., and Liébault, F. (2010).
920 Assessment of intermediate fine sediment storage in a braided river reach
921 (southern french prealps). *Hydrological Processes*, 24:1318–1332.
- 922 Némery, J., Mano, V., Coynel, A., Etcheber, H., Moatar, F., Meybeck, M.,
923 Belleudy, P., and Poirel, A. (2013). Carbon and suspended sediment trans-
924 port in an impounded alpine river (Isère, France). *Hydrological Processes*.
- 925 Newcombe, C. P. and Macdonald, D. D. (1991). Effects of suspended sedi-
926 ments on aquatic ecosystems. *North American Journal of Fisheries Man-
927 agement*, 11:72–82.
- 928 Olivier, A., Pierrefeu, G., Scotti, M., and Blanquart, B. (2008). Incerti-
929 tude sur les débits calculés à partir des courbes de transformation hau-
930 teur/débit (Uncertainty associated with discharges computed from stage
931 discharge relationships). In *Hydrological measurements and uncertainties,
932 SHF conference (in French)*, Paris, France.
- 933 Olsen, N. (1999). Two-dimensional numerical modelling of flushing processes
934 in water reservoirs. *Journal of Hydraulic Research*, 37:3–16.
- 935 Peteuil, C., Fruchard, F., Abadie, F., Reynaud, S., Camenen, B., and Guer-
936 tault, L. (2013). Sustainable management of sediment fluxes in reservoir
937 by environmental friendly flushing: the case study of Gèniissiat dam on
938 upper Rhône River (France). In *Proc. 13th International Symposium on
939 River Sedimentation*.
- 940 Petticrew, E. L., Krein, A., and Walling, D. E. (2007). Evaluating fine
941 sediment mobilization and storage in a gravel-bed river using controlled
942 reservoir releases. *Hydrological Processes*, 21:198–210.
- 943 Petts, G. E. and Gurnell, A. M. (2005). Dams and geomorphology: Research
944 progress and future directions. *Geomorphology*, 71:27–47.
- 945 Rayan, R. C. and Iguacel, C. M. (2006). Effects of flushing of two reservoirs
946 in Spain. In *Proc. 3rd River Flow conference*.
- 947 Ryan, R. J. and Boufadel, M. C. (2006). Incomplete mixing in a small, urban
948 stream. *Journal of Environmental Management*, 81:50–57.

- 949 Serlet, A. J., Gurnell, A. M., Zolezzi, G., Wharton, G., Belleudy, P., and
950 Jourdain, C. (2018). Biomorphodynamics of alternate bars in a chan-
951 nelized, regulated river: An integrated historical and modelling analysis.
952 *Earth Surface Processes and Landforms*, 43(9):1739–1756.
- 953 Smart, G. M. (1999). Barrage flushing implications (monitoring sediment
954 releases from the Rangipo hydro barrage). In *Proc. 28th IAHR Congress*,
955 Graz.
- 956 Tena, A., Vericat, D., and Batalla, R. (2014). Suspended sediment dynamics
957 during flushing flows in a large impounded river (the lower river ebro, ne
958 iberian peninsula). *Journal of Soils and Sediments*.
- 959 Thollet, F., Camenen, B., Le Coz, J., NÃ©mery, J., and Rousseau, C.
960 (2018). Measurements of the fine sediment fluxes in the arvan, arc, and
961 isère rivers [suivi du transport sédimentaire sur les rivières arvan, arc et
962 isère]. Technical report, INRAE/ENSE3/IGE. (in French).
- 963 Van Maren, S., Yang, M., and Wang, Z. (2010). Predicting the morpho-
964 dynamic response of silt-laden rivers to water and sediment release from
965 reservoirs: Lower Yellow River, China. *Journal of Hydraulic Engineering*,
966 137:90–99.
- 967 Vörösmarty, C. J., Meybeck, M., Fekete, B., Sharma, K., Gree, P., and
968 Syvitski, J. P. M. (2003). Anthropogenic sediment retention: major global
969 impact from registered river impoundments. *Global and Planetary Change*,
970 39(1):169 – 190. The supply of flux of sediment along hydrological path-
971 ways: Anthropogenic influences at the global scale.
- 972 Wohl, E. E. and Cenderelli, D. A. (2000). Sediment deposition and transport
973 patterns following a reservoir sediment release. *Water Resources Research*,
974 36:319–333.
- 975 Yoon, Y. N. (1992). The state and the perspective of the direct sedimenta-
976 tion removal methods from reservoirs. *International Journal of Sediment*
977 *Research*, 7:99–115.